ORGANIC PROCESS RESEARCH & DEVELOPMENT
OPR&D
Article
Cite This: Org. Process Res. Dev. 2018, 22, 707−720
pubs.acs.org/OPRD

Continuous Production of Anhydrous *tert*-Butyl Hydroperoxide in Nonane Using Membrane Pervaporation and Its Application in Flow Oxidation of a γ-Butyrolactam

Bryan Li,*[,†] Steven M. Guinness,[†] Steve Hoagland,[†] Michael Fichtner,[†] Hui Kim,[†] Shelly Li,[†] Robert J. Maguire,[†] J. Christopher McWilliams,[†] Jason Mustakis,[†] Jeffrey Raggon,[†] Dan Campos,[‡] Chris. R. Voss,[‡] Evan Sohodski,[‡] Bryan Feyock,[‡] Hannah Murnen,[‡] Miguel Gonzalez,[§] Matthew Johnson,[§] Jiangping Lu,[§] Xichun Feng,[§] Xingfang Sun,[§] Songyuan Zheng,[§] and Baolin Wu[§]

[†]Pfizer Worldwide Research and Development, Eastern Point Road, Groton, Connecticut 06340, United States
[‡]Compact Membrane Systems, 335 Water Street, Newport, Delaware 19804, United States
[§]Asymchem Life Science (Tianjin) Co., Ltd., No. 71 Seventh Avenue, TEDA, Tianjin 300457, China

ABSTRACT: Anhydrous *tert*-butyl hydroperoxide (TBHP) is a powerful oxidizing agent in many chemical transformations. Despite the versatility in organic reactions, the use of anhydrous TBHP has been greatly limited because of safety concerns over its shipping, handling, and storage, particularly on production scale. Herein we describe a membrane pervaporation method that allows the production of the anhydrous TBHP solution in continuous manner. The system consists of membrane modules in series that are made of perfluorinated polymer with very high gas permeability, allowing it to remove water efficiently. The pervaporation skid has been successfully implemented in production by continuously generating anhydrous 1.5 M TBHP solution in nonane at a rate of up to 100 mL·min^{-1} for more than 96 h, achieving the target of 0.15 wt % water. An integrated flow oxidation of a γ-butyrolactam substrate provides an efficient and diastereoselective synthesis of a key lactam intermediate for the preparation of a drug candidate targeting interleukin-1 receptor associated kinase 4 for the treatment of inflammation and oncology diseases.

1. INTRODUCTION

Interleukin-1 receptor associated kinase 4 (IRAK4) is a serine threonine kinase that serves as a key node in innate immune signaling and is activated by the interleukin 1 (IL-1) family receptors (IL-1R, IL-18R, and IL-33R) as well as the Toll-like receptors (TLRs). Inhibition of IRAK-4 blocks the production of inflammatory cytokines such as type-I interferons, IL-6, tumor necrosis factor (TNF), IL-1, and IL-12 that are key drivers of autoimmune and inflammatory diseases. IRAK4 is an attractive therapeutic target for diseases associated with dysregulated inflammation, such as systemic lupus erythematosus (SLE) and rheumatoid arthritis.[1] Compound **1**[2] (Scheme 1) is a potent and selective IRAK4 inhibitor currently under clinical development. The complexity of the active pharmaceutical ingredient (API) synthesis arises primarily from chiral lactam **2** featuring three contiguous stereocenters. In the early generation of the synthesis, **2** was prepared from electrophilic fluorination of its precursor **4a** via enolation followed by reaction with *N*-fluorobenzenesulfonimide (Scheme 2). The reaction gave a mixture of diastereomers of **5** and **6**; the undesired trans isomer **5** was the major product in a ∼2:1 ratio to the desired cis isomer **6**. In addition, the difluorinated byproduct **7** was typically observed at the ∼5% level.[3] To make the matter further complicated, the lactam **4a** precursor was contaminated with ∼5% **4b** as an impurity[4] that equally participated in the reaction to give the corresponding

Scheme 1. Retrosynthesis of IRAK4 Inhibitor 1

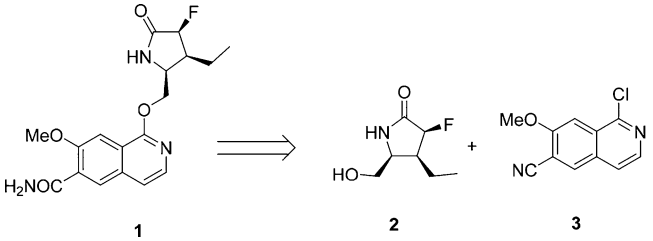

1 2 3

Scheme 2. Early Synthesis of α-Fluorolactam 2[a]

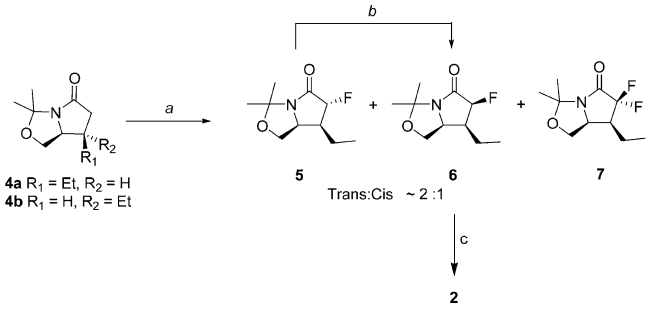

[a]Reagents and conditions: (a) LDA, NFSI, THF, −78 °C. (b) LDA, THF, −20 °C. (c) TFA, MeCN/water.

Received: March 20, 2018
Published: May 23, 2018

DOI: 10.1021/acs.oprd.8b00083
Org. Process Res. Dev. 2018, 22, 707−720

fluorinated isomers as impurities. The desired product had to be isolated by silica gel chromatography,[5] a challenging and laborious task that consumed a large amount of silica gel and solvents. The undesired isomer **5** from the chromatographic isolation was then subjected to epimerization under basic conditions to equilibrate to give a ∼ 1:1 mixture of **5** and **6** at best. After workup, the resulting mixture was again chromatographed to yield a second crop of the desired isomer **6**. The recycle was typically repeated one more time to give an overall yield of 28−35%[6] for this single chemical transformation step (**4a** → **6**). In an API campaign, for the preparation of 14 kg of **6**, ∼30 000 L of solvents and ∼600 kg of silica gel were used for the chromatography operation alone. Furthermore, the isolated product from the chromatographic isolation and one recrystallization[5] was still contaminated with difluorinated and unreacted materials at levels of 0.5−1.0%. As the clinical development of **1** advanced to phase II and a large quantity of the API was needed, it became evident that a more efficient synthesis was needed.

2. RESULTS AND DISCUSSION

We envisioned that a diastereoselective synthesis through the preparation of hydroxylated lactam **8a** would be viable. Nucleophilic substitution at the α-carbon can often be achieved with high retention of stereointegrity.[7] α-Oxidations of ketones, carboxylic esters, and lactams are well-known in the literature.[8] When the enolate of **4a** was reacted with oxygen at −78 °C, the diastereoselectivity was only ∼4:1 (**8a**/**8b**). Use of Vedejs reagent or other peroxides[9] was not considered because of high cost and difficulty of production. Subsequently we turned our attention to hydroxylation of carbanions via the transfer of an electrophilic oxygen atom.[10] In this approach, lithium *tert*-butyl peroxide (LiOO*t*Bu), which is readily generated from LDA or LHMDS and *tert*-butyl hydroperoxide (TBHP), is reacted with a carbanion to give the hydroxylated product.[11] Using this method, we found that a highly diastereoselective hydroxylation of **4a** could be achieved in an **8a**/**8b** ratio greater than 30:1 (Scheme 3). With this finding, we set out to understand the reaction kinetics and impurity profiles under different conditions.

ReactIR was used to monitor the progression of both the enolate formation and the oxidation reaction. While it was difficult to generate definitive trends that correlated to the consumption of LiOO*t*Bu, the disappearance of the 1693 cm^{-1} IR band corresponding to the carbonyl stretch of **4a** and the appearance of the enolate double-bond stretch at 1611 cm^{-1} were found to be suitable for monitoring the enolate formation. In turn, the disappearance of the 1611 cm^{-1} absorbance and growth of the band at 1686 cm^{-1} corresponding to the product **8a** were used to monitor the oxidation (Figure 1). In early studies, LHMDS (2.2 equiv) was added to a solution of **4a** in THF slowly over a 1 h period to maintain the internal temperature at −70 °C. The enolate formation was rapid, as evidenced by the IR trend (Figure 1). After the enolate was completely formed, anhydrous TBHP solution was added to the reaction mixture at −70 °C. No reaction was observed at −70 °C, and the reaction mixture was warmed gradually to −30 °C, whereupon the formation of **8a** was detected by the appearance of the band at 1686 cm^{-1} (Figure 2). The reaction was sluggish at this temperature, and further warming to −5 °C enabled the reaction to reach the "desired" completion point (vide infra). As the reaction was observed to give rise to an overoxidized byproduct, the diketo compound **9**, the optimal reaction quench point to maximize the yield was not at full conversion of **4a** but rather at the conversion where there was a balance between **9** and the unreacted starting material **4a**. In the ReactIR-monitored run, we tested the addition of a 5 mol % excess of TBHP at the 05:10 time point (Figure 3) and noticed a drop in the total area of the 1686 cm^{-1} IR absorbance from 2.0 to an area value of 1.8 over the following 40 min. At 06:00, an additional 5% LHMDS was introduced, which increased the 1686 cm^{-1} band, returning the total area of this absorbance back to 2.0. This was interpreted and confirmed by UPLC offline analysis that excess TBHP could lead to the increase of **9**, and the additional base could drive the conversion of **4a** further. With the understanding that the reaction was sluggish at −30 to −20 °C, we compared the reaction outcomes using three different addition orders: (1) adding TBHP to the preformed enolate at −70 °C and warming to −20 °C; (2) adding TBHP to the enolate at −20 °C; and (3) adding LHMDS to the mixture of **4a** and TBHP at −20 °C, allowing all reactions to warm to 0 °C over 2 h. The reaction profiles for the head-to-head runs were nearly identical, giving product **8a** in 80−82% in situ yield with the diastereoselectivity consistently at >30:1 and major impurities **4a** and **9** at less than 5%. After reaction quench and workup, the crude product could be converted to **6** directly by reaction with XtalFluor-E. Alternatively, it was treated with triflic anhydride in the presence of 2,6-lutidine to give triflate **10** as an intermediate, which underwent S_N2 fluorination with triethylamine trihydrogen fluoride to give **6** as the product. Triflate **10** appeared to be sufficiently stable to undergo aqueous extractive workup and was carried forward as a solution into the fluorination reaction. The reactions proceeded with no loss of stereointegrity. With the crude product at >80 area % UPLC purity, the isolation of **6** could be accomplished by crystallization from *n*-heptane. The overall yield (**4a** → **6**) was in the range of 40−50% after factoring in the potency of the starting material without chromatography. This represented a substantial process improvement from the early synthesis by greatly reducing the production time and process waste as a consequence of the elimination of the recycling of **5**, extensive chromatography, and the distillation of thousands of liters of solvent. With this chemistry in place, the next challenge was to turn it into a viable process. Not surprisingly, the focal point for further development of the process was the supply and/or generation of anhydrous TBHP.

Scheme 3. Improved Synthesis of 6 Using the Oxenoid Approach[a]

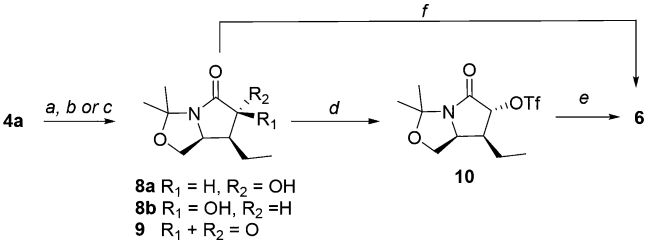

[a]Reagents and conditions: (a) **4a,** LHMDS (2.2 equiv), THF, −70 °C, then dry air, −70 °C → 0 °C. (b) **4a,** LHMDS (2.2 equiv), THF, −70 °C, then TBHP, −70 °C → 0 °C. (c) **4a** and TBHP, −20 °C, then LHMDS (2.2 equiv), −20 °C → 0 °C. (d) Tf_2O, 2,6-lutidine, DCM, 0 °C. (e) TEA·3HF, TEA, 2-MeTHF. (f) XtalFluor-E, 2-MeTHF, 40 °C.

DOI: 10.1021/acs.oprd.8b00083
Org. Process Res. Dev. 2018, 22, 707−720

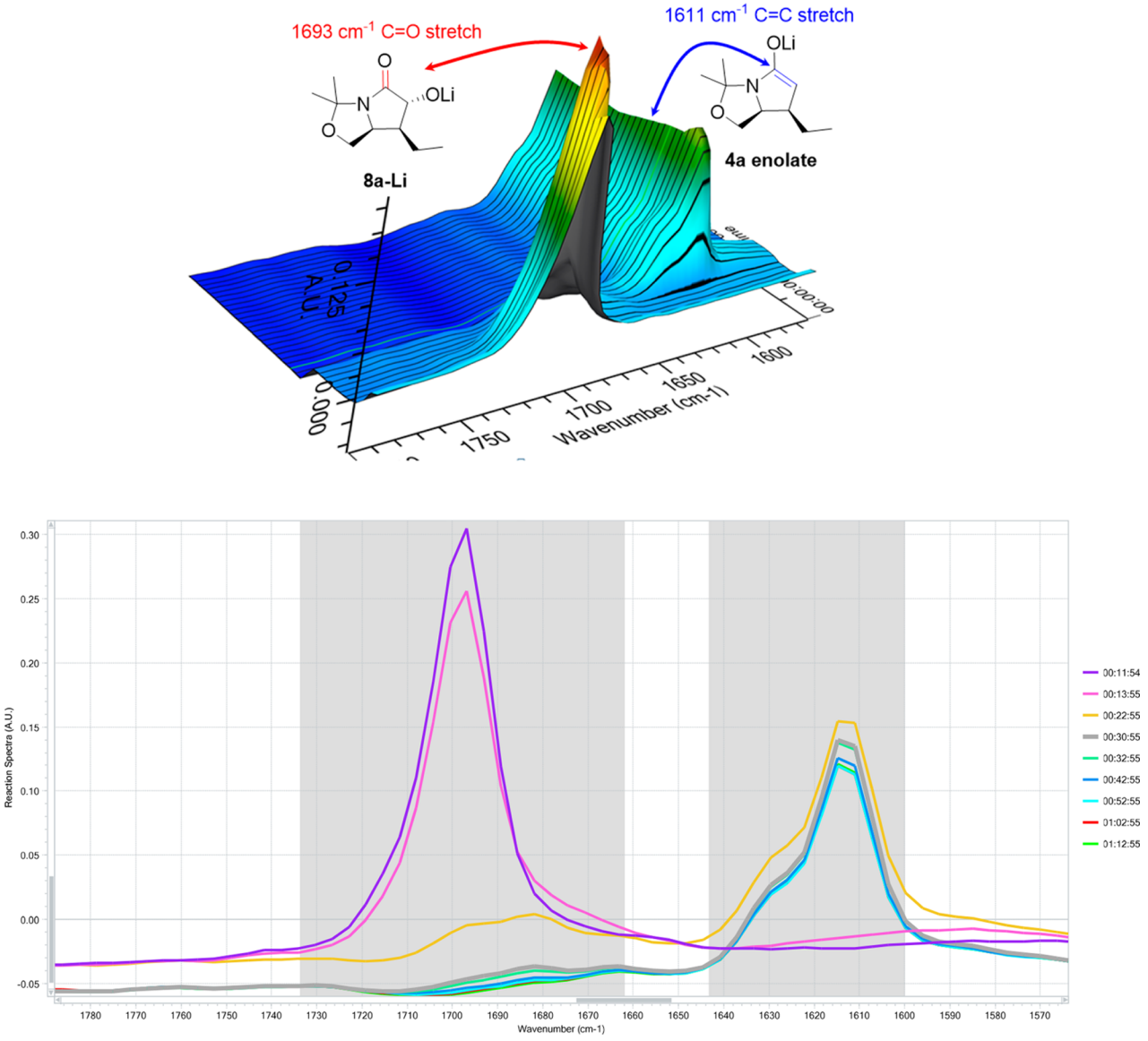

Figure 1. Trends of the IR bands at 1693 and 1611 cm^{-1} during enolate formation.

3. ANHYDROUS TBHP MEMBRANE PERVAPORATION

3.1. TBHP and Its Safety. Anhydrous TBHP is a powerful oxidizing agent in many chemical transformations.[12] Its use in Sharpless epoxidation[13] is probably the most well-known and practiced application in organic synthesis. More recently, anhydrous TBHP under Cu(II) catalysis was used for the preparation of highly functionalized benzylic esters, α-keto amides, and propargylamines.[14] Despite the versatility in organic reactions, the use of anhydrous TBHP has been greatly limited because of safety concerns associated with shipping, handling, and storage, particularly at production scale. A serious explosion[15] occurred during the engineering development of a Sharpless epoxidation process when TBHP was dried by azeotropic distillation using the published procedure.[16] The explosion was believed to be caused by inadvertent heating of a very concentrated TBHP solution.[15] Another accident involving TBHP occurred in 2007 in a chemical company in China and led to two deaths and four injuries.[17] Consequently, the production of anhydrous TBHP in both the laboratory and production setting is much discouraged. For small-scale laboratory use, anhydrous TBHP solution in hydrocarbons[18] is commercially available. Nevertheless, because of the explosive risk in transportation and storage, anhydrous TBHP is not available on bulk scale and has been largely avoided by the community of process chemists for scale-up use. On the other hand, 70 wt % TBHP solution in water (TBHP-70AQ), an important reagent in the polymer industry, is readily available in bulk quantities, as its explosion hazards have been evaluated extensively from laboratory-scale to intermediate-scale tests.[19] Though TBHP-70AQ also presents serious safety concerns, the thermal stability data of TBHP-70AQ suggested that the exothermic onset temperature of TBHP is 69.5 °C.[20] Liu and co-workers suggested that TBHP-70AQ must be controlled below 55.6 °C to ensure safety during production, transportation and storage.[17] In addition, it should be noted that TBHP appears to be very sensitive to minor impurities and traces of metals.[21]

Because of safety concerns over storage of large volumes of anhydrous TBHP solution, it is advantageous to maintain a relatively small inventory of the reagent, as this minimizes the accumulation of potential energy that can be released at one

DOI: 10.1021/acs.oprd.8b00083
Org. Process Res. Dev. 2018, 22, 707−720

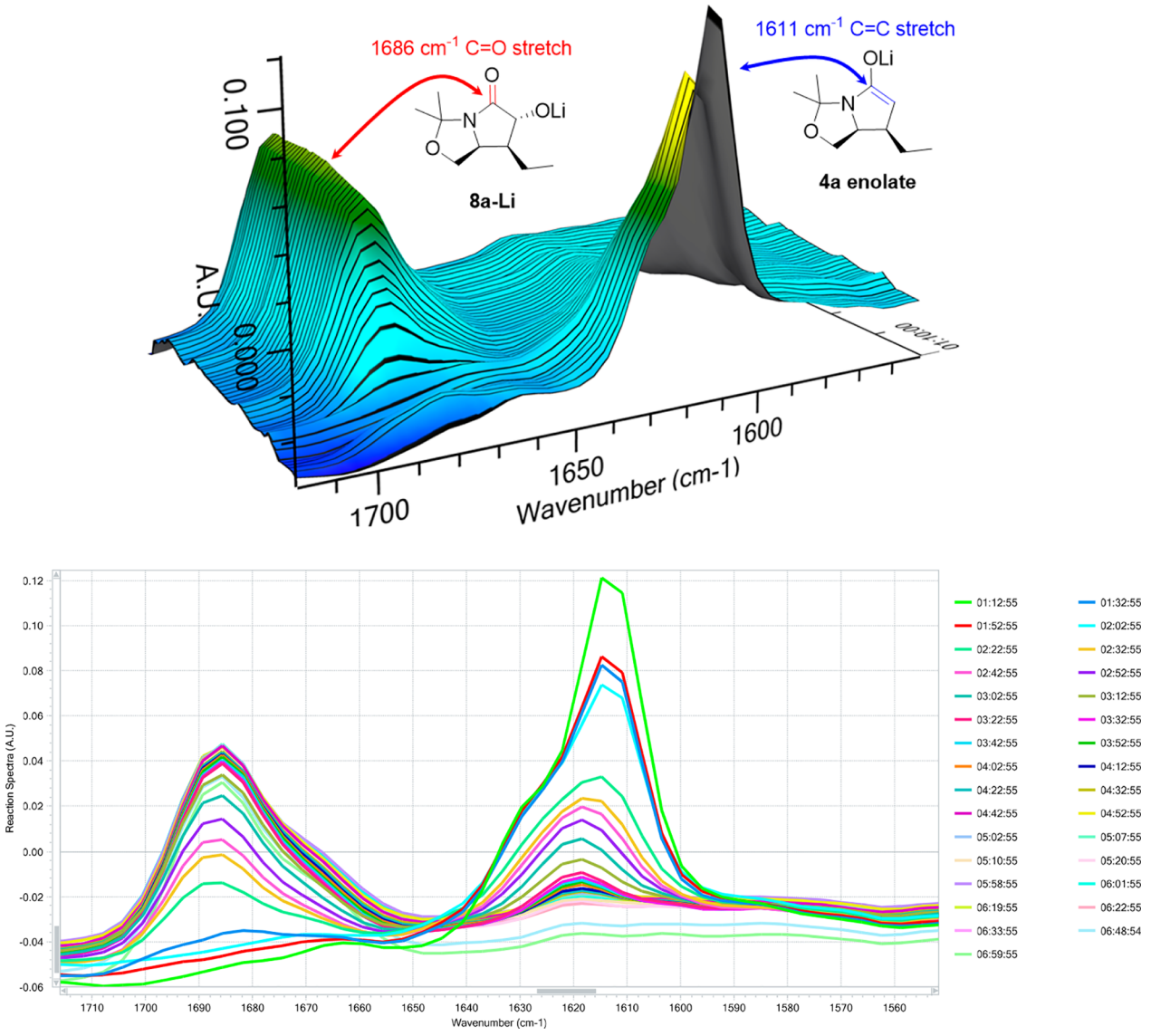

Figure 2. Trends of the IR bands at 1686 and 1611 cm^{-1} during the oxidation reaction.

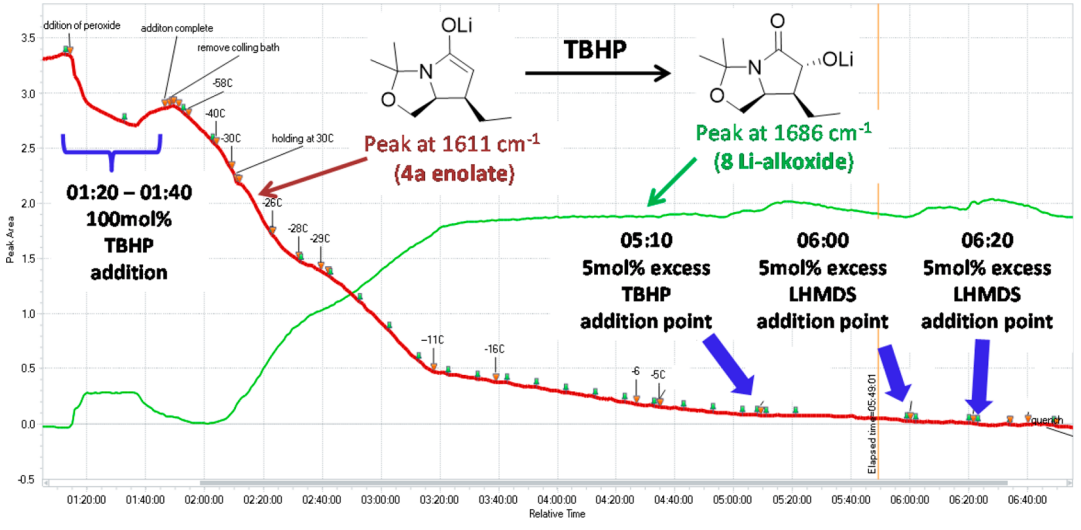

Figure 3. Trends of the IR bands at 1686 and 1611 cm^{-1} after TBHP addition.

DOI: 10.1021/acs.oprd.8b00083
Org. Process Res. Dev. 2018, 22, 707−720

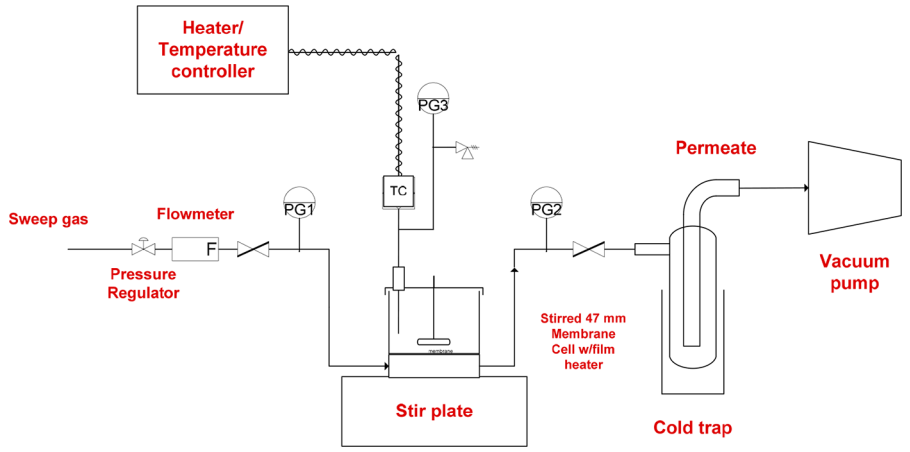

Figure 4. Laboratory stirred-cell pervaporation system.

time. Consequently, continuous processing presents inherent advantages, wherein the generation of anhydrous TBHP solution is followed by the consumption of the reagent within a short time. However, the execution of a continuous drying process for TBHP was without precedent. An azeotropic drying method was deemed unsafe, as the distillation temperature of 70−75 °C under reduced pressure to remove water through its azeotrope with toluene would exceed the differential scanning calorimetry (DSC) degradation onset point. The use of dehydrating agents such as anhydrous magnesium sulfate, sodium sulfate, and molecular sieves was also considered. However, in a continuous drying operation, the use of solid drying agent(s) in cartridges or vessels would require a large TBHP holdup volume. A more serious concern was the exothermicity of the drying process and the difficulty in controlling the solution temperature within a continuous drying apparatus. The life span of the drying agent(s) would also require close monitoring, in addition to the generation of solid wastes. An attractive approach to water removal from organic solvents is the use of membrane pervaporation (PV) technology, which generates minimal waste, has a low operating cost, and most importantly does not generate heat. In a recent pharmaceutical application, PV technology was piloted as a green process for the recovery of THF in manufacturing.[22] With that precedent, the Pfizer team engaged Compact Membrane Systems, Inc. (CMS) to test and develop PV drying of TBHP.

3.2. Membrane Pervaporation Drying Studies and System Design. Small-scale laboratory PV tests were designed to determine the kinetics of drying a 1.5 M solution of TBHP in nonane[23] containing up to 1 wt % water. The tests were conducted with a laboratory-scale PV system, shown schematically in Figure 4. This unit consists of a cell loaded with a 47 mm membrane disk. The lab-scale membrane consists of a thin composite membrane with a perfluorinated polymer coated on top of a chemically and thermally resistant microporous flat-sheet support. The cell was loaded with the TBHP/nonane mixture, where it was stirred and heated to a target temperature. Vacuum was applied on the permeate side for a predetermined length of time. At the end of the test, the remaining solution in the cell and the permeate captured in the cold trap were weighed and analyzed by Karl Fischer (KF) titration to determine the water concentration. The lab test results are summarized in Table 1. Five tests were run, each starting with 8 g of the initial mixture. To minimize the concentration of TBHP in the permeate, the tests were run with an inert gas sweep rate of 100 $cm^3 \cdot min^{-1}$.

Table 1. Lab Tests Results on the Pervaporation of TBHP/Nonane

test no.	run time (min)	temperature (°C)	permeate pressure (psia)	H_2O content by KF (wt %) initial	final
1	180	24	0.2	0.90	0.10
2	150	24	0.2	0.86	0.12
3	151	27	0.9	0.66	0.09
4	102	32	1.2	0.82	0.09
5	82	35	1.2	0.86	0.12

The water permeance of the membrane does not depend on the liquid feed composition. However, the water permeation rate per unit area or flux is a function of the liquid feed composition and temperature, membrane area, and vacuum (or permeate pressure) according to the following relationship:

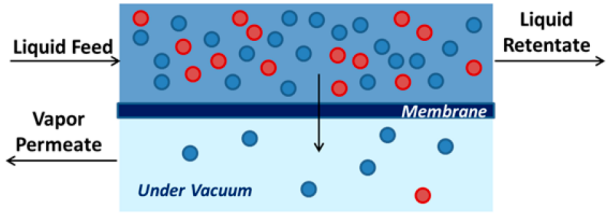

$$Q_w = \frac{\pi}{\delta}(\gamma\, x\, P^o - p\, y)$$

where Q_w is the water flux (in $mol \cdot (cm^2 \text{ of membrane})^{-1} \cdot s^{-1}$), x is the water mole fraction of the permeating species in the bulk of the liquid feed, π is the water permeability (in $mol \cdot cm^{-2} \cdot s^{-1} \cdot cmHg^{-1} \cdot \mu m^{-1}$), γ is the water activity coefficient under the liquid feed conditions, P° is the water vapor pressure (in cmHg), p is the permeate pressure (in cmHg), and y is the water mole fraction in the permeate.

The water/organic (TBHP) separation factor was about 360, which means that the permeation rate of water is much greater than that of the organic. The separation factor of water relative to the organic is given by the following expression:

$$SF_{W-O} = (X_{W,P}/X_{W,F})/(X_{O,P}/X_{O,F})$$

where SF_{W-O} is the water−organic separation factor, $X_{W,P}$ is the mass fraction of H_2O in the permeate, $X_{W,F}$ is the mass fraction

DOI: 10.1021/acs.oprd.8b00083
Org. Process Res. Dev. 2018, 22, 707−720

Table 2. Water Permeability–Activity Coefficient Product, $\pi\gamma$, As Calculated Using Data and the Pervaporation Model

	$\pi\gamma$ in various units		
test no.	molar flow (mol·μm·s^{-1}·cm^{-2}·cmHg^{-1})	standard gas flow (std cm^3·μm·s^{-1}·cm^{-2}·cmHg^{-1})	membranologist units (barrer)
1	3.90×10^{-7}	0.0087	8728
2	4.03×10^{-7}	0.0090	9017
3	3.44×10^{-7}	0.0077	7705
4	4.09×10^{-7}	0.0091	9147
5	3.92×10^{-7}	0.0088	8780
avg.	**3.88×10^{-7}**	**0.0087**	**8675**

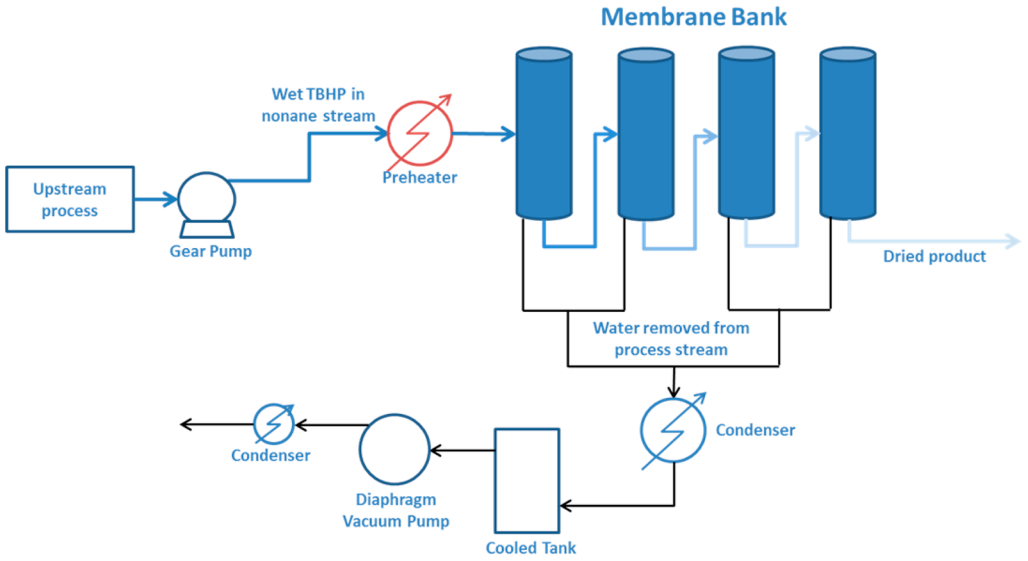

Figure 5. Flow diagram of the skid-mounted PV system for continuous drying of 1.5 M TBHP/nonane.

of H_2O in the feed, $X_{O,P}$ is the mass fraction of organic in the permeate, and $X_{O,F}$ is the mass fraction of organic in the feed.

A mass balance around the system in Figure 4 yields the following simplified model for the batch pervaporation:

$$\ln \frac{x_i}{x_f} = \frac{\pi\gamma A P^\circ}{m\delta} t$$

where x_i and x_f are the initial and final water mole fractions, respectively, A is the membrane area (in cm^2), m is the number of moles of TBHP/nonane mixture, δ is the membrane thickness (in μm), and t is the time (in s).

Using the data from Table 1 in the model above, the fundamental parameter for the process was determined: the permeability–activity coefficient product, $\pi\gamma$. The values of $\pi\gamma$ for each of the tests of Table 1 are shown in Table 2. It should be noticed that within the measurement error, $\pi\gamma$ is basically independent of temperature and concentration in the respective ranges studied for these factors. Since this parameter is independent of whether the system is run in batch or continuous mode, it could be used to design the skid-mounted continuous pervaporation system to achieve the main goal of this project (vide infra).

Using the data from the batch process study, a scale-up skid-mounted PV system was designed and constructed. The PV system was specifically designed for continuous drying of up to 100 mL of the mixture per minute at a feed temperature between 40 to 45 °C. Sufficient membrane surface area was supplied to obtain a dry product containing no more than 0.20 wt % water. A simplified flow diagram of the PV system is shown in Figure 5. The incoming feed is preheated between 40 and 45 °C and then enters a bank of four membrane modules with the feed connected in series. The retentate from module 1 becomes the feed of module 2; the retentate from module 2 becomes the feed of module 3, and so on. The retentate from module 4 is the dried product. The system provides the means for intermembrane stage heating to maintain a nearly constant temperature in the feed to each module. Water from the feed to each module selectively permeates through the membrane. Some organics also permeate through the membrane. However, the permeability of the organics (TBHP and nonane) is substantially lower than that of water (<1:360). The permeate streams from each module, which are in the vapor phase, are mixed and directed to a condenser and then collected as a liquid in the permeate tank (cooled tank in Figure 5). The permeate tank is kept under vacuum by the vacuum pump and maintained at low temperature by a cooling coil.

Membrane Modules. The membrane modules used in the skid are commercially produced by CMS. The modules consist of a membrane cartridge and a housing. The membrane cartridge is made from a perfluorinated polymer (active layer) coated on hundreds of microporous hollow fibers made of a thermally and chemically resistant material. The cartridges are contained in a special stainless steel (SS) housing. A picture of the cartridge and housing is shown in Figure 6.

3.3. Adaptation to a Continuous Flow Process. With the realization of a continuous drying process for the safe generation of anhydrous TBHP, the continuous consumption of TBHP to minimize total accumulation was the second part of the solution. As the safe handling and storage of anhydrous TBHP was the primary objective to enable the key stereo-

DOI: 10.1021/acs.oprd.8b00083
Org. Process Res. Dev. 2018, 22, 707–720

Figure 6. Commercial CMS membrane cartridge and housing

selective lactam oxidation step, continuous flow technology emerged as the optimal choice for the process. Continuous processing technology offers many advantages over batch methods, including precise control of stoichiometry, reaction time, and temperature, high reproducibility, and often better reaction yields.[24] The much higher surface area to volume ratio under flow conditions allows highly efficient heat transfer. When coupled with the much smaller volume in the reaction train, safety hazards in handling exothermic reactions associated with explosive intermediates are minimized.[25]

The oxidation reaction of **4a** works effectively when **4a** and TBHP are combined, then LHMDS is added at −20 °C, and then the temperature is allowed to rise to −5 to +5 °C to drive the reaction to completion (vide supra). This batch process was found to be readily adaptable to continuous processing. Extensive research and development (R&D) was conducted to obtain the optimal parameters for the production campaigns. The R&D work was extended to upstream operational units, where an aqueous TBHP solution was first extracted in nonane using a continuous extractor and the resulting water-saturated TBHP/nonane solution was continuously dehydrated using pervaporation. A total of >200 kg of **4a** has been processed to date (Table 3), and a fully continuous TBHP extraction and dehydration and lactam oxidation process was implemented in the last campaign. Modifications to the equipment setup and process conditions were found to be necessary to realize the fully continuous process, which led to an improvement in the overall yield and purity (vide infra).

The equipment setup and process parameters used to deliver the first ∼12 kg of **8a** are depicted in Figure 7. The TBHP/nonane solution was extracted in batch mode, dehydrated using the PV system, and then mixed with **4a** and THF in a 500 L glass-lined reactor to obtain the reagent solution (vide infra). The initial process conditions for the oxidation utilized two streams (**4a**/TBHP/nonane and LiHMDS solutions) that were fed to a plug flow reactor (PFR)/continuous stirred tank reactor (CSTR) hybrid system. The PFR was oriented in a vertical position with a planned residence time of 75 min, and the three CSTRs in series were expected to give an additional residence time of 30 min. This flow setup was expected to give the desired reaction end point. The fourth CSTR was used for continuous quenching of the residual TBHP; workup was performed in batch mode.

A reload campaign of ∼2 times the size quickly followed after the first delivery. Some modifications were made in order to reduce the equipment footprint and optimize the process. The size of the PFR was increased to 50 L, and the number of CSTRs was reduced to one, as depicted in Figure 7. Tables 4 and 5 provide comparisons of the different reactors used.

The oxidation reaction was evaluated to optimize its residence time and streamline the equipment by potentially eliminating the CSTR downstream of the PFR. Two experiments were conducted with similar feed rates while the configuration of the reactors was varied as follows: experiment no. 1 with the regular setup of one PFR and one CSTR in series and experiment no. 2 with only one PFR for the oxidation reaction. Because of the reduction in residence time resulting from elimination of the downstream CSTR, an additional 30 min was added to the PFR residence time for a total reaction time of 90 min. The reaction conditions were kept consistent, and only the reaction setup was modified as described previously. Experiment no. 1 (PFR + CSTR) provided less starting material (**4a** = 0.07%; **8a** = 80.31%; **9** = 8.33%), while experiment no. 2 (PFR only) exhibited a higher concentration of unreacted **4a** (∼4.62%) despite the longer residence time.

The higher length/diameter ratio (L/D) in the 50 L PFR reduces axial dispersion and promotes radial dispersion, thereby enhancing the conversion by approximating an ideal PFR. Because of the increase in reactant flow rates to accommodate higher throughput, the mean velocity is higher; nevertheless, the laminar flow regime (Reynolds number (Re) < 2100) is maintained, and mixing of the reactants is governed by diffusion in the radial direction with reduced axial dispersion. Implementation of a larger PFR to increase throughput was deemed to be low risk on the basis of the aforementioned factors, and it was validated during the campaign by producing consistent-quality material. Also, the downstream CSTRs were evaluated to streamline equipment setup while maintaining similar reaction profile. Table 5 depicts the optimized parameters based on the evaluation results to reduce the three CSTRs used in campaign 1 to a proposed single CSTR in campaign 2. A similar mixing pattern was achieved by keeping

Table 3. Campaign Summary

campaign no.	manufacturing mode			output of **8a**		
	TBHP extraction	TBHP/nonane drying by pervaporation	oxidation reaction (residence time)	potency-corrected weight (kg)	HPLC purity (%)	yield (%)
1	batch	flow (90 mL·min^{-1})	flow PFR (30 L), three CSTR (8 L each) (115 min)	12.2	80.4	72.6
2	batch	flow (90 mL·min^{-1})	flow PFR (50 L), one CSTR (50 L) (90 min)	31.0	80.0	71.8
3	flow (105 mL·min^{-1})	flow (90 mL·min^{-1})	flow PFR (50 L), one CSTR (20 L) (90 min)	148.6	84.2	75.9

DOI: 10.1021/acs.oprd.8b00083
Org. Process Res. Dev. 2018, 22, 707−720

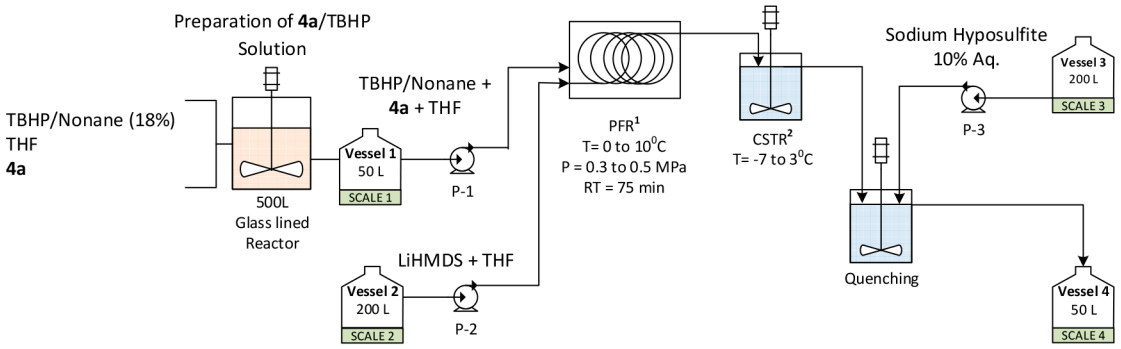

Figure 7. Process flow diagram for the oxidation reaction and quenching step.

Table 4. Comparison of PFR Parameters at Three Scales

scale	D (mm)	L/D	reactor volume (L)	cross-sectional area (mm^2)	mean velocity ($mm \cdot min^{-1}$)	residence time (min)	Re
lab	2.14	46 729	0.360	3.6	1329	75.2	74
campaign 1	15	10 667	28.27	176.6	2278	70	885
campaign 2	15	20 000	53.01	176.6	4099	73	1593

Table 5. Continuous Stirred Tank Reactor Comparison

scale	reactor volume (L)	residence time (min)	impeller type	construction material	heat transfer fluid (HTF)	HTF flow rate ($L \cdot min^{-1}$)	jacket volume (L)
campaign 1	24 (three 8 L CSTRs)	40	propeller	316SS	ethanol	8	5
campaign 2	50 (one *50 L* CSTR)	20	propeller	glass	ethanol	8	10

Table 6. Process Conditions and Results for Integration of the Pervaporation and Reaction Systems

		IPC results (%)		
entry	reaction conditions[a]	**4a**	**8a**	**9**
1	A: **4a** + TBHP (1.1 equiv) + THF (24 $mL \cdot g^{-1}$; 2.96 $g \cdot min^{-1}$) B: LiHMDS (1 M; 3.23 $g \cdot min^{-1}$)	2.2	85.6	6.0
2	A: **4a** + THF (15 $mL \cdot g^{-1}$; 1.86 $g \cdot min^{-1}$) B: TBHP (1.1 equiv; 0.46 $g \cdot min^{-1}$) C: LiHMDS (1 M; 5 equiv; 2.97 $g \cdot min^{-1}$)	2.5	71.1	11.4
3	A: **4a** + THF (7.5 $mL \cdot g^{-1}$; 1.01 $g \cdot min^{-1}$) B: TBHP (1.1 equiv) + THF (7.5 $mL \cdot g^{-1}$; 1.31 $g \cdot min^{-1}$) C: LiHMDS (1 M; 5 equiv; 1.97 $g \cdot min^{-1}$)	1.3	86.2	8.0

[a]Residence times: PFR, 60 min; CSTR, 40 min.

the same type of impeller and equivalent reactor geometry at different scales.

The experimental data demonstrated that the reaction could be completed using only a single CSTR in lieu of three CSTRs with a reduced residence time (20 min). A larger CSTR (50 L) combines the nominal working volume of the three CSTRs and provides the advantage of allowing steady-state dynamics to be reached sooner, thereby streamlining the equipment setup. Experiments were performed in an attempt to remove the CSTR and complete the reaction solely in the PFR. While similar product purities were achieved, the reaction profiles were different, and full conversion of **4a** was not achieved in the PFR-only setup. The data suggest that while more **4a** is converted to the product in the CSTR, there is also simultaneous conversion of the product to the diketone impurity **9**. The reaction profile afforded by utilizing the CSTR is preferred since **9** can be purged in downstream steps while residual starting material is more difficult to remove and impacts the overall yield. Understanding the kinetics of the oxidation reaction and diketone impurity formation may be helpful in understanding the dynamics in each of the reactors and further optimizing the process to possibly enable a single PFR reactor to be used.

In both campaigns 1 and 2, extraction of the TBHP solution was carried out as a batch process. This was clearly undesirable, as it would require the storage of multihundred liters of anhydrous TBHP solution. In addition, the original process premixed **4a** solution in THF with the anhydrous TBHP/nonane solution, and it was held as one of the two feed streams. Though it was deemed safe on the basis of process safety testing, precombining an ethereal solvent with a peroxide solution is not considered a good practice. Thus, a continuous extraction of the aqueous TBHP solution was developed to avoid the accumulation of large volumes of anhydrous TBHP

DOI: 10.1021/acs.oprd.8b00083
Org. Process Res. Dev. 2018, 22, 707−720

solution and the premixing of TBHP and THF solutions. Three different experiments (entries 1−3) were performed using a typical "T-mixer" to investigate the new addition order prior to the oxidation reaction. Process conditions and results are summarized in Table 6. Experimental data (entry 3) demonstrated that it was important to dilute the TBHP/nonane solution with THF, and a simple inline mixing between the reaction solutions was found to be effective and to provide similar results as premixing in the 500 L reactor (entry 1). Additional types of static mixers were then evaluated to determine the best type for the production campaign.

Evaluation of Mixing Efficiency of the Oxidation Reaction Feed Solutions Using Inline Static Mixers. Seven different types of mixers, ranging from T-Mixers to inline agitators and tube-in-tube jets, were evaluated to determine the optimal setup for large-scale production. The different mixers used in this study are summarized in Table 7.

Table 7. Inline Mixers Summary (4a in THF + TBHP/Nonane Solution)

		IPC results (%)		
mixer	description	4a	8a	9
1	T-mixer; same diameter inlet/outlet	6.0	80	3.0
2	T-mixer; smaller inlet diameter, bigger outlet diameter	4.5	81	7.5
3	T-mixer; smaller inlet diameter, bigger outlet diameter with SS packing in the outlet coil	3.3	81	4.4
4	inline mixer with mechanical agitator	2.8	85	7.0
5	inline mixer without agitator but with SS packing in the agitator housing	1.1	83	5.5
6	tube-in-tube cocurrent jet mixer	1.8	80	9.0
7	tube-in-tube countercurrent jet mixer	1.4	81	6.0

In-process control (IPC) samples were collected at the outlets of the PFR and the CSTR to measure the presence of **4a**, **8a**, and **9** in order to understand the impact of mixing in the oxidation reaction.

An ideal reaction profile would give high **8a** purity and low residuals of **4a** and **9**. Since the starting material **4a** is more difficult to purge in the downstream chemistry but the diketone impurity **9** can be readily rejected, residual **4a** was a primary factor in the evaluation of the inline mixers. On the basis of the analytical results, the three best mixers are (a) the inline mixer with mechanical agitator, (b) the inline mixer without a mechanical agitator but with SS packing on the agitator's housing, and (c) the tube-in-tube countercurrent jet mixer. In consideration of manufacturing of the mixer and simplicity/robustness in operation (e.g., fewer moving parts), the project team decided to implement the tube-in-tube countercurrent jet mixer.

Pervaporation System Performance and Integration of Process Analytical Technology at Production Scale. The pervaporation system has been utilized in three separate campaigns and for continuous operations up to 96 h. The KF analysis results for the anhydrous TBHP solution were consistent at 1100 ± 200 ppm. Figure 8 shows the PV system at the kilo lab facility, where it continuously dehydrated the TBHP/nonane solution to support campaigns 1 and 2. For campaign 3, the portable PV system was moved to the pilot plant to support the larger-scale manufacturing. This pervaporation system was connected to the extraction and reaction systems (upstream and downstream operational units, respectively) to enable end-to-end processing of extraction/drying/oxidation. The connection of the pervaporation unit to the reaction system also reduced the risk of tetrahydrofuran peroxide generation, which had been identified as a potential safety risk associated with the premixing of the TBHP/nonane and starting material/THF solutions. Figure 9 presents the process flow diagram showing the interconnectivity between the different operational units as set in campaign 3.

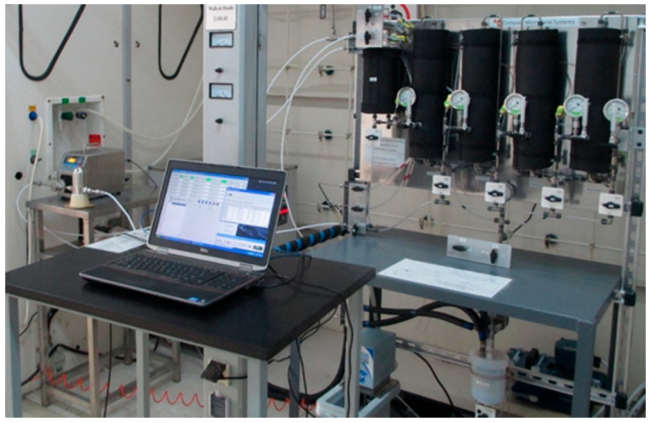

Figure 8. Pervaporation system at the kilo lab facility

PV Performance in Scale-Up Runs. On a typical run, the "wet" TBHP/nonane solution (water content ∼1% by KF) was fed to the pervaporation system at a rate of 65 g·min^{-1} to provide enough residence time throughout the four membrane modules to reduce the water content to less than 0.15 wt %. The system was sampled every 1−3 h, and if the solution failed to reach the KF target, then the feed rate was adjusted accordingly to provide a longer residence time for the dehydration process. The material not meeting the KF criteria could be recirculated through the system for further KF reduction, and therefore, no waste was generated. When the PV system operated without telescoping to the downstream units (e.g., the oxidation reaction), as occurred in campaigns 1 and 2, the material was collected in SS drums[26] and then manually transferred. The material collected in the drums was assayed for water content by KF analysis and TBHP content by NMR analysis. In campaign 1, the anhydrous TBHP solution in nonane was collected in four drums; the KF results ranged from 798−1230 ppm, and the TBHP potency was 16.68−17.13%.

As the campaign size increased by more than 12-fold in the third campaign, large volume storage of TBHP was not a preferred option, and an integrated continuous process was desired. This required the TBHP solution entering the oxidation reaction to meet both the specifications of dryness and concentration. Thus, process analytical technology using ReactIR was investigated to monitor the TBHP concentration at the outlet of the PV system. A calibration curve was established, and the data were collected throughout campaign 3. The results were compared with the TBHP content measured by NMR analysis. Adjustments of the reagent flow rates in the downstream oxidation reaction were performed manually, but the results from the IR monitoring demonstrated the feasibility of using ReactIR for automated adjustments in the future. Figure 10 shows the characteristic IR calibration curve used in campaign 3. A calibration curve was generated using TBHP standards to correlate the TBHP concentration (wt %) and the IR peak area.

DOI: 10.1021/acs.oprd.8b00083
Org. Process Res. Dev. 2018, 22, 707−720

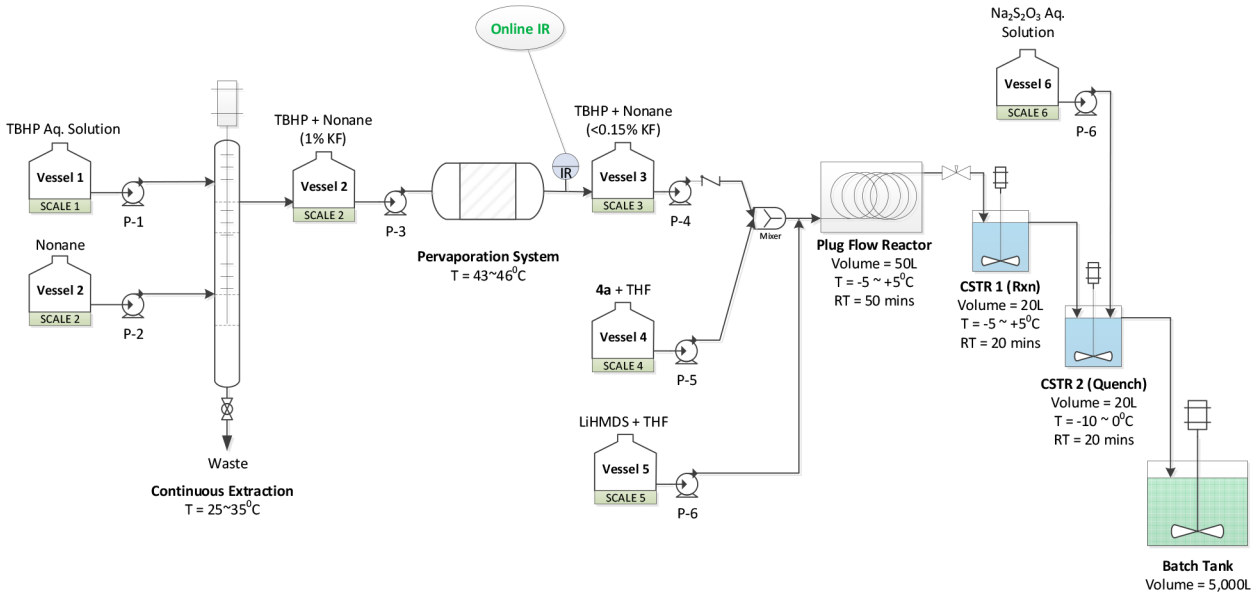

Figure 9. Campaign 3 process flow diagram.

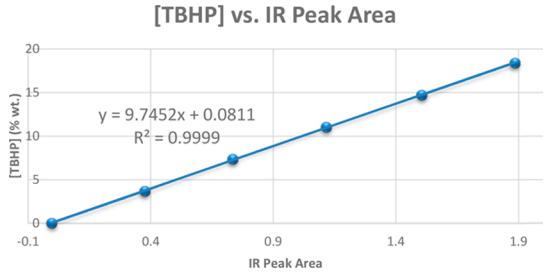

Figure 10. IR calibration curve for TBHP concentration.

From the calibration curve and average IR peak area data collected for all four runs in campaign 3, the TBHP concentrations were calculated. Figure 11 shows IR peak area data for a 24 h monitoring period. The average IR peak area during that period was 1.65−1.7, which equated to a TBHP concentration of approximately 16.4 wt % based on the system calibration curve. The step change in TBHP concentration close to the mark of 36 000 s (Figure 11) was attributed to a change in the continuous extraction system where the starting material solution was slightly more concentrated but still within the operating range.

Samples were periodically retrieved to measure the TBHP concentration via NMR analysis. The average NMR [TBHP] values were compared with [TBHP] values obtained from the IR instrument (see Figure 12 for details).

The average concentration of TBHP measured by IR on all four batches was 16.4 wt %, and the concentration measured by NMR was 16.7 wt %. The difference between the two analytical methods, 0.3 wt %, equated to 0.02 equiv of TBHP, which was insignificant given the 20% excess of TBHP used in the reaction. Thus, the online IR method provided a high level of confidence in monitoring the TBHP concentration.

The improved synthetic route combined with the application of continuous manufacturing delivered a safer process as well as

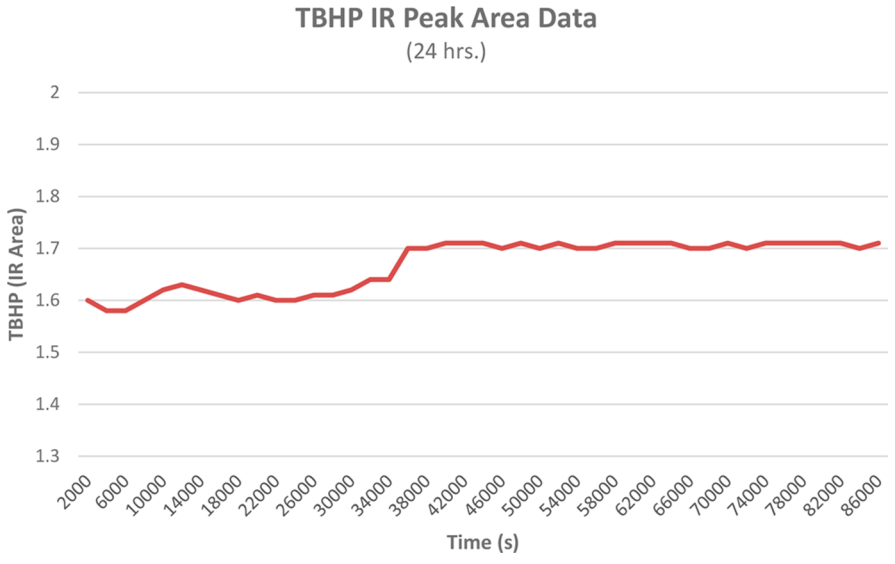

Figure 11. TBHP IR peak area information collected at the PV system outlet

DOI: 10.1021/acs.oprd.8b00083
Org. Process Res. Dev. 2018, 22, 707−720

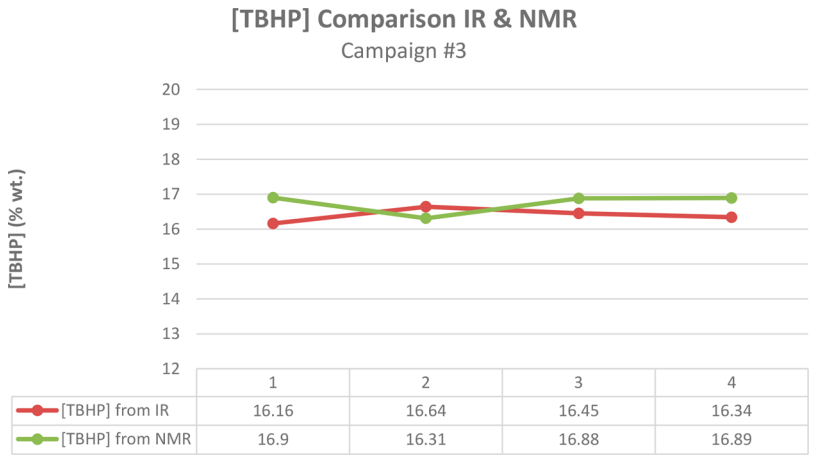

Figure 12. Comparison of [TBHP] data obtained from IR and NMR analyses.

reducing waste. Impact on the environment was measured by the calculated E-factor. The E-factor calculated for the previous synthetic route was 1948, while that for the improved chemistry in flow was 131, a 15-fold reduction.[27] Continuous improvements and modifications to the process are ongoing to deliver an end-to-end flow process encompassing all operational units through product isolation.

4. SUMMARY

We have developed an alternative, scalable method for the continuous preparation of anhydrous TBHP solution. The continuous PV drying method for TBHP is run at a temperature below the DSC decomposition onset, well-controlled, and reproducible, and it generates the anhydrous TBHP solution on demand, thereby avoiding a large stockpile volume typically encountered in batch processes. The PV skid with four 2 in. commercial modules was used to continuously generate anhydrous 1.5 M TBHP solution at a rate of up to 100 $mL \cdot min^{-1}$ for more than 96 h in a single run. With the implementation of the PV drying, the large-scale continuous oxidation of **4a** to support the API campaign of IRAK4 inhibitor **1** has become feasible. To the best of our knowledge, this also represents the first example of using anhydrous TBHP solution in the production of pharmaceutical intermediates.

EXPERIMENTAL SECTION

General Information. ^1H NMR spectra were recorded in $CDCl_3$ using a Varian Mercury Plus 400 MHz spectrometer; the chemical shifts are reported in parts per million in reference to $CDCl_3$ (7.26 ppm for ^1H NMR and 77.0 ppm for ^{13}C NMR). The online IR spectrum for TBHP dehydration was recorded on a Bruker MATRIX-MF explosion-proof spectrometer equipped with an IN350-T ATR-Fiber (MIR) accessory. The batch reaction development used ReactIR iC10 by Mettler Toledo. UPLC analysis was performed using a Waters Acquity HSS T3 column (1.8 μm, 2.1 mm × 50 mm) on a Waters H-Class UPLC chromatograph with photodiode array detector and autosampler. HPLC-grade acetonitrile and trifluoroacetic acid were purchased from commercial sources. Water used for preparing the mobile phase was purified using a Milli-Q 10A ultrapure water system. UPLC method: mobile phase A, 0.05% TFA in H_2O; mobile phase B, MeCN; flow rate, 0.65 $mL \cdot min^{-1}$; column temperature, 30 °C; detection at 210 nm; injection volume, 1 μL; run time, 9 min; gradient: t = 0 min, 5% B; 6.9 min, 100% B; hold at 100% B for 1.5 min; ramp to 5% B in 1.5 min.

Caution! *Although the continuous TBHP drying process was carried out successfully in a scale-up facility without incident, our experience has been limited only to the handling of 1.5 to 2.0 M TBHP solution in nonane. Extreme caution should be exercised in handling TBHP solutions of any strength, and users should refer to recommended practices in the literature and from the commercial suppliers.*[28]

Continuous Production of (6*R*,7*S*,7a*S*)-7-Ethyl-6-hydroxy-3,3-dimethyltetrahydro-3*H*,5*H*-pyrrolo[1,2-*c*]-oxazol-5-one (8a). *Feed Solutions Preparation and/or Staging.* The following solutions were prepared:

Solution A: 134.6 kg of nonane.

Solution B: 44.8 kg of aqueous 70 wt % TBHP (note: for safety, the amount of TBHP on the production floor was limited to 50 L at any point in time).

Solution D: A clean, dry 3000 L glass-lined reactor was evacuated (vacuum of approximately −0.05 to −0.08 MPa) and then filled with nitrogen until the oxygen content was less than 1.0% (0.2% O_2). While a temperature between 20 and 30 °C (23.4−24.7 °C) was maintained, 996.8 kg of THF was added to the reactor, followed by 46.5 kg (corrected for potency) of **4a**, and the mixture was stirred for 1−2 h (102 min).

Solution F: 1022 kg (209.6 corrected) of lithium bis-(trimethylsilyl)amide in THF.

Solution G: In a 1000 L glass-lined reactor kept at a temperature between 20 and 30 °C, 46 kg of sodium thiosulfate was mixed in 414 kg of purified water.

Continuous Extraction of TBHP. A glass extraction column with 316SS discs was swept with nitrogen for 0.5−1 h, and the oxygen content was measured to ensure that it was below 1% (0.9%). While a temperature of 25−35 °C was maintained, 4.6 kg of solution A (nonane) and 1.5 kg of solution B were added to the column. Solutions A and B were continuously added to the column at rates of 20 and 60 $g \cdot min^{-1}$ respectively. The flow rate of each solution was monitored and controlled using a setup of electronic scales and pumps managed by a programmable logic controller (PLC). The TBHP/nonane solution (solution C) with water content of ∼1% was continuously discharged from the top of the column and collected in a 50 L

DOI: 10.1021/acs.oprd.8b00083
Org. Process Res. Dev. 2018, 22, 707−720

SS vessel. The aqueous phase from the bottom of the column was collected, analyzed, and discarded.

Pervaporation (TBHP/Nonane Dehydration). The pervaporation system bath temperature was set to 48−53 °C for the heat-up cycle and then controlled at 43−46 °C (44.1 °C) for the process; vacuum was controlled at −28 inHg by means of a dedicated vacuum pump. Solution C was continuously added at a rate of 65 g·min^{-1} using a similar feed setup as for the continuous extraction, in which a PLC was used to monitor and control the flow rate. The dehydrated TBHP/nonane solution was collected in a 50 L SS vessel and assayed for TBHP content via NMR spectroscopy (15.8−17.3 wt %) before being fed to the next operational unit (reaction). The solution (solution E) was also sampled from the outlet of the PV system every 4−12 h, for the water content to be below 1500 ppm (average of 1127 ppm) as determined by KF analysis.

Reaction and Quenching. A 50 L 316SS PFR and a two 20 L 316SS CSTRs were cooled to between −7 and −3 °C. The PFR temperature was controlled at −7 to −3 °C and the temperature of the CSTRs at −5 to 5 °C. The PFR was swept with nitrogen for 30 min, and then 50.1 kg of THF was pumped into the PFR to test the stability of the automatic feed system and ensure dryness (H_2O < 500 ppm by KF) of the system prior to the reaction (H_2O = 130 ppm by KF). CSTR1 was used to complete the reaction, while CSTR2 was used for continuous quenching with solution G. A downstream 5000 L glass-lined reactor, whose temperature was controlled at −10 to 0 °C, was set as a reservoir of the quenched solution in preparation for workup.

All of the feed solutions were controlled with the following flow rates in the automatic feed control system: solution D (**4a** solution) = 409 g·min^{-1}; solution E (TBHP/nonane solution) = 60 g·min^{-1}; solution F (LiHMDS solution) = 373 g·min^{-1}; solution G (quenching solution) = 170 g·min^{-1}. It should be noted that solution G was started once the reaction solution started to overflow from CSTR1. After 100 min, the quenched solution from CSTR2 was sampled for purity analysis by UPLC, and then it was sampled every 1−3 h for **4a** < 2 area % (**4a** = 0 area %). The overall reaction time was set to 70 min (50 min in the PFR, 20 min in the CSTR). After the addition was completed, 50.1 kg of THF was pumped into the PFR to push out the reaction solution, followed by a nitrogen sweep into the receiving reactor.

Workup and Isolation. Once all of the quenched solution was collected into the 5000 L glass-lined reactor, the pH of the mixture was adjusted with a solution of concentrated HCl (149.8 kg) and water (370.0 kg) at a rate of 10−40 kg·h^{-1} (addition time of 7 h 43 min) and a temperature of −5 to 5 °C. After the whole aqueous HCl solution had been added, the mixture was stirred for 25 min, and the pH was checked to be between 8 and 9. Following the pH adjustment, the mixture was warmed to 20−30 °C under stirring and nitrogen sparging. The reaction mixture was sampled every 2−4 h to confirm that the pH was in the range of 7−8. After 10 h, the mixture was sampled and analyzed by GC (wt %) for the presence of residual hexamethyldisilazane (HMDS) until it reached ≤0.05%. Sodium chloride (115 kg) was added to the reactor, and the phases were allowed to settle. The organic phase was transferred to another reactor, and the aqueous phase was extracted with 2-MeTHF (2 × 391 kg). The combined organic phase was concentrated to a volume of ∼500 L ($T \leq 45$ °C, $P \leq -0.09$ MPa) and then filtered and rinsed with THF (20.0 kg). The desired product solution (143.3 kg of solution, 37.8 kg after correction by assay; 74.9% yield, 82% purity by UPLC with detection at 210 nm) was carried forward to downstream steps directly. An analytically pure sample was obtained by chromatography as a light-yellow oil. ^{1}H NMR ($CDCl_3$, δ) 4.41−4.35 (1H, m), 4.09 (1H, d, J = 3.3 Hz), 3.95 (1H, dd, J = 5.8 and 8.3 Hz), 3.88−3.73 (1H, m), 3.55 (1H, dd, J = 8.3 and 10.3 Hz), 2.23 (1H, qd, J = 7.7 and 4.4 Hz), 1.63 (s, 3H), 1.55−1.44 (5H, m), 1.02 (3H, t, J = 7.4 Hz). ^{13}C NMR ($CDCl_3$, δ) 172.43, 91.59, 79.84, 64.87, 61.37, 41.83, 26.94, 23.52, 21.47, 12.33. MS: calcd for $C_{10}H_{18}NO_3^+$ (M + 1) 200.1; found 200.1, 142.0.

(6*S*,7*S*,7a*S*)-7-Ethyl-6-fluoro-3,3-dimethyltetrahydro-3*H*,5*H*-pyrrolo[1,2-*c*]oxazol-5-one (6). *Method 1.* To a reaction flask was added XtalFluoro-E (1.30 equiv, 28.4 mmol, 6.84 g), and 2-MeTHF (50 mL) was added. The mixture was cooled to 0 °C, and triethylamine trihydrofluoride (1.35 equiv, 29.5 mmol, 4.80 g) was added. No exotherm was observed. Triethylamine (2.33 equiv, 50.9 mmol, 5.15 g) was added dropwise while the temperature of the mixture was kept below 10 °C (the addition was exothermic). **8a** (5.0 g, 21.8 mmol) was added as a solution in 2-MeTHF (25 mL). The addition was slightly exothermic. After the addition, the reaction mixture was heated at 30 °C for 2 h and then cooled to 15 °C. Disodium hydrogen phosphate (1 M in water; 2 equiv, 43.7 mL) was added. The layers were separated, and the aqueous phase was extracted one more time with 2-MeTHF (10 volumes). The combined organic phase was concentrated to ∼25 mL, filtered through a silica gel pad (10 g, 200 wt %) in a fritted funnel, and rinsed with 150 mL of 40% EtOAc in heptane. The filtrate was vacuum-concentrated to an oil and stirred with 25 mL of heptane at 20 °C. After 2 h of stirring, the resulting slurry was filtered. The filter cake was pulled dry under vacuum and then dried in a vacuum oven to give 3.18 g of the desired product (64% yield) with 99.16% UPLC purity (210 nm) as a white solid. ^{1}H NMR ($CDCl_3$, δ) 5.23 (dd, 1H, J = 51.6 and 7.3 Hz), 4.18−4.00 (m, 1H), 3.76−3.64 (m, 1H), 2.71−2.63 (m, 1H), 1.78−1.68 (m, 5H), 1.48 (s, 3H), 1.44−1.28 (m, 1H), 0.96 (t, 3H, J = 7.3 Hz). ^{13}C NMR ($CDCl_3$, δ) 165.48 (d, J = 23.4 Hz), 93.22 (s), 91.37 (d, J = 24.0 Hz), 84.74 (s), 58.12 (d, J = 2.2 Hz), 41.90 (d, J = 16.8 Hz), 26.29 (s), 24.41(s), 15.50 (d, J = 8.8 Hz), 12.82 (d, J = 2.9 Hz).

Method 2. To a reaction flask were added **8a** (5.0 g, 25.1 mmol) and dichloromethane (50 mL). 2,6-Lutidine (1.5 equiv, 37.641 mmol, 4.03 g) was added, and the resulting solution was cooled to −5 °C. Trifluoromethanesulfonic anhydride (1.2 equiv, 30.12 mmol, 8.50 g) was added dropwise while the temperature was kept below 0 °C. After 10 min, the reaction was confirmed to be complete by UPLC analysis of a reaction aliquot. The reaction was quenched with water (50 mL), and the mixture was allowed to warm to >5 °C during the water addition. The phases were separated. The DCM phase was solvent-exchanged with 2-MeTHF (125 mL) to a final volume of ∼50 mL (20 °C, 50 mmHg). The triflate in the 2-MeTHF solution was then treated with 2,6-lutidine (3 equiv, 75.3 mmol, 8.07 g) at 20 °C.

Triethylamine trihydrofluoride (1.5 equiv, 37.64 mmol, 6.19 g) was added dropwise to the mixture while the temperature was kept under 20 °C (the pH of the reaction mixture was about 5). After 3 h, the reaction was determined to be complete as assayed by UPLC. Water (50 mL) was added. The mixture was stirred and settled, and the aqueous phase was removed. The organic phase was washed with 10% citric acid solution and then vacuum-concentrated (35 °C, 40 mmHg) to give a

DOI: 10.1021/acs.oprd.8b00083
Org. Process Res. Dev. 2018, 22, 707−720

brown oil, which failed to crystallize. Thus, the oil was stirred with 25 g of silica gel in the presence of 2% TEA in MTBE (100 mL) for 2 h and filtered. The filter cake was washed with MTBE (200 mL). The filtrate was vacuum-concentrated to an oil, which was stirred with heptane (50 mL). Crystallization occurred upon seeding with 3 mg of the product. After 2 h of granulation, the solids were collected with a Buchner funnel and rinsed with heptane (10 mL). Drying gave 3.03 g of the desired product (60% yield) with ~97% UPLC purity (210 nm). The spectroscopic data were identical to those for the material obtained from method 1.

AUTHOR INFORMATION

Corresponding Author

*E-mail: bryan.li@pfizer.com.

ORCID

Bryan Li: 0000-0002-7972-9966

J. Christopher McWilliams: 0000-0002-4764-735X

Notes

The authors declare no competing financial interest.

ACKNOWLEDGMENTS

The authors thank Drs. Jean Beebe and Katherine Lee for suggestions in the preparation of the manuscript.

REFERENCES

(1) (a) Chaudhary, D.; Robinson, S.; Romero, D. L. Recent Advances in the Discovery of Small Molecule Inhibitors of Interleukin-1 Receptor-Associated Kinase 4 (IRAK4) as a Therapeutic Target for Inflammation and Oncology Disorders. *J. Med. Chem.* **2015**, *58*, 96−110. (b) Hynes, J., Jr.; Nair, S. K. Advances in the discovery of small-molecule IRAK4 inhibitors. *Annu. Rep. Med. Chem.* **2014**, *49*, 117−133. (c) Seganish, W. M. Inhibitors of interleukin-1 receptor-associated kinase 4 (IRAK4): a patent review (2012−2015). *Expert Opin. Ther. Pat.* **2016**, *26*, 917−932. (d) Wang, Z.; Wesche, H.; Stevens, T.; Walker, N.; Yeh, W.-C. IRAK-4 inhibitors for inflammation. *Curr. Top. Med. Chem.* **2009**, *9*, 724−737.

(2) Lee, K. L.; Ambler, C. M.; Anderson, D. R.; Boscoe, B. P.; Bree, A. G.; Brodfuehrer, J. I.; Chang, J. S.; Choi, C.; Chung, S.; Curran, K. J.; Day, J. E.; Dehnhardt, C. M.; Dower, K.; Drozda, S. E.; Frisbie, R. K.; Gavrin, L. K.; Goldberg, J. A.; Han, S.; Hegen, M.; Hepworth, D.; Hope, H. R.; Kamtekar, S.; Kilty, I. C.; Lee, A.; Lin, L. L.; Lovering, F. E.; Lowe, M. D.; Mathias, J. P.; Morgan, H. M.; Murphy, E. A.; Papaioannou, N.; Patny, A.; Pierce, B. S.; Rao, V. R.; Saiah, E.; Samardjiev, I. J.; Samas, B. M.; Shen, M. W. H.; Shin, J. H.; Soutter, H. H.; Strohbach, J. W.; Symanowicz, P. T.; Thomason, J. R.; Trzupek, J. D.; Vargas, R.; Vincent, F.; Yan, J.; Zapf, C. W.; Wright, S. W. Discovery of Clinical Candidate 1-{[(2S,3S,4S)-3-Ethyl-4-fluoro-5-oxopyrrolidin-2-yl]methoxy}-7-methoxyisoquinoline-6-carboxamide (PF-06650833), a Potent, Selective Inhibitor of Interleukin-1 Receptor Associated Kinase 4 (IRAK4), by Fragment-Based Drug Design. *J. Med. Chem.* **2017**, *60*, 5521−5542.

(3) By UPLC with detection at a wavelength of 210 nm.

(4) Choi, C.; Nuhant, P.; Mousseau, J. J.; Yang, X.; Gerstenberger, B. S.; Williams, J. M.; Wright, S. W. Synthesis of Chiral Azabicycles from Pyroglutaminols. *Org. Lett.* **2016**, *18*, 5748−5751.

(5) Both **4a** and **4b** are oils, and purification at the precursor stage was not deemed feasible. Both **5** and **6** are low-melting solids when obtained in pure form, but isolation of either **5** or **6** by crystallization was not attainable without chromatographic purification first. However, it was possible to enhance the product purity by recrystallization from *n*-heptane.

(6) The combined chromatographed material had to be further crystallized to achieve the desired purity, which further reduced the overall yield.

(7) (a) Lowe, G.; Potter, B. V. L. Synthesis, absolute configuration, and circular dichroism of the enantiomers of fluorosuccinic acid. *J. Chem. Soc., Perkin Trans. 1* **1980**, *9*, 2029−2032. (b) Bresciani, S.; O'Hagan, D. Stereospecific benzylic dehydroxyfluorination reactions using Bio's TMS-amine additive approach with challenging substrates. *Tetrahedron Lett.* **2010**, *51*, 5795−5797. (c) Shiuey, S. J.; Partridge, J. J.; Uskokovic, M. R. Triply convergent synthesis of 1.alpha.,25-dihydroxy-24(R)-fluorocholecalciferol. *J. Org. Chem.* **1988**, *53*, 1040−1046. (d) Avent, A. G.; Bowler, A. N.; Doyle, P. M.; Marchand, C. M.; Young, D. W. Stereospecific Synthesis of 4-Fluoroglutamic Acids. *Tetrahedron Lett.* **1992**, *33*, 1509−1512.

(8) (a) Sparks, S. M.; Chow, C. P.; Zhu, L.; Shea, K. J. Type 2 Intramolecular N-Acylnitroso Diels-Alder Reaction: Scope and Application to the Synthesis of Medium Ring Lactams. *J. Org. Chem.* **2004**, *69*, 3025−3035. (b) Hamed, O. A.; El-Qisairi, A.; Qaseer, H.; Hamed, E. M.; Henry, P. M.; Becker, D. P. Asymmetric α-hydroxy ketone synthesis by direct ketone oxidation using a bimetallic palladium(II) complex. *Tetrahedron Lett.* **2012**, *53*, 2699−2701. (c) Adam, W.; Metz, M.; Prechtl, F.; Renz, M. Facile *Synthesis* of α-Hydroxy Amides and Esters by Direct Autoxidation of Their Titanium Enolates. *Synthesis* **1994**, *1994*, 563−566. (d) Sunden, H. H.; Engqvist, M.; Casas, J.; Ibrahem, I.; Cordova, A. Direct Amino Acid Catalyzed Asymmetric α Oxidation of Ketones with Molecular Oxygen. *Angew. Chem., Int. Ed.* **2004**, *43*, 6532−6535. (e) LaPorte, T. L.; Hamedi, M.; DePue, J. S.; Shen, L.; Watson, D.; Hsieh, D. Development and Scale-Up of Three Consecutive Continuous Reactions for Production of 6-Hydroxybuspirone. *Org. Process Res. Dev.* **2008**, *12*, 956−966.

(9) (a) Vedejs, E. A Method for Direct Hydroxylation of Enolates. Transition Metal Peroxide Reactions. *J. Am. Chem. Soc.* **1974**, *96*, 5944−5946. (b) Vedejs, E.; Larsen, S. Hydroxylation of Enolates with Oxodiperoxymolybdenum(pyridine)(hexamethylphosphoric triamide), MoO_5·Py·HMPA(MoOPh): 3-Hydroxy-1,7,7-trimethylbicyclo[2.2.1]heptan-2-one. *Org. Synth.* **1986**, *64*, 127−135. (c) Wang, P.-S.; Zhou, X.-L.; Gong, L. Z. An Organocatalytic Asymmetric Allylic Alkylation Allows Enantioselective Total Synthesis of Hydroxymetasequirin-A and Metasequirin-B Tetramethyl Ether Diacetates. *Org. Lett.* **2014**, *16*, 976−979.

(10) (a) Julia, M.; Pfeuty-Saint-Jalmes, V.; Plé, K.; Verpeaux, J.-N.; Hollingworth, G. Hydroxylation of Carbanions with Lithium *tert*-Butylperoxide Acting as an Oxenoid. *Bull. Soc. Chim Fr.* **1996**, *133*, 15−24. (b) Julia, M.; Saint-Jalmes, V. P.; Verpeaux, J.-N. Oxidation of Carbanions with Lithium tert-Butyl Peroxide. *Synlett* **1993**, *1993*, 233−234. (c) Castro, B. Existence and Stability of *gem*-Alkoxy Organomagnesium Compounds. I. *Bull. Soc. Chim. Fr.* **1967**, 1533−1540.

(11) Minko, Y.; Marek, I. Oxenoids in organic synthesis. *Org. Biomol. Chem.* **2014**, *12*, 1535−1546.

(12) (a) Han, G. L.; Zhang, Q.; Zhong, J.; Shao, H.; Zhang, H. R. Separation of Dimethylformamide/H_2O Mixtures Using Pervaporation−Distillation Hybrid Process. *Adv. Mater. Res.* **2011**, *233-235*, 866−869. (b) Liu, Y.; Tsunoyama, H.; Akita, T.; Tsukuda, T. Efficient and selective epoxidation of styrene with TBHP catalyzed by Au_{25} clusters on hydroxyapatite. *Chem. Commun.* **2010**, *46*, 550−552. (c) Singhal, S.; Jain, S. L.; Prasad, V. V. D. N.; Sain, B. An Environmentally Friendly Oxidation System for the Selective Oxygenation of Aldimines to Oxaziridines with Anhydrous TBHP and Alumina-Supported MoO_3 as a Recyclable Heterogeneous Catalyst. *Eur. J. Org. Chem.* **2007**, *2007*, 2051−2054. (d) Jain, S. L.; Joseph, J. K.; Sain, B. Alumina supported MoO_3: an efficient and recyclable catalyst for selective oxidation of tertiary nitrogen compounds to *N*-oxides using anhydrous TBHP as oxidant under mild reaction conditions. *Catal. Lett.* **2007**, *115*, 8−12.

(13) (a) Hanson, R. M.; Sharpless, K. B. Procedure for the catalytic asymmetric epoxidation of allylic alcohols in the presence of molecular sieves. *J. Org. Chem.* **1986**, *51*, 1922−1925. (b) Gao, Y.; Hanson, R. M.; Klunder, J. M.; Ko, S. Y.; Masamune, H.; Sharpless, K. B. Catalytic asymmetric epoxidation and kinetic resolution: modified procedures including in situ derivatization. *J. Am. Chem. Soc.* **1987**, *109*, 5765−5780. (c) Wang, Z. M.; Zhou, W. S. Asymmetric epoxidation of allylic

DOI: 10.1021/acs.oprd.8b00083
Org. Process Res. Dev. 2018, 22, 707−720

alcohol by the modified Sharpless reagent. *Tetrahedron* **1987**, *43*, 2935−2944. (d) Qian, Q.; Tan, Y.; Zhao, B.; Feng, T.; Shen, Q.; Yao, Y. Asymmetric Epoxidation of Unsaturated Ketones Catalyzed by Heterobimetallic Rare Earth−Lithium Complexes Bearing Phenoxy-Functionalized Chiral Diphenylprolinolate Ligand. *Org. Lett.* **2014**, *16*, 4516−4519. (e) Jeon, S.-J.; Li, H.; Walsh, P. J. A Green Chemistry Approach to a More Efficient Asymmetric Catalyst: Solvent-Free and Highly Concentrated Alkyl Additions to Ketones. *J. Am. Chem. Soc.* **2005**, *127*, 16416−16425. (f) Kakei, H.; Tsuji, R.; Ohshima; Shibasaki, T. M. Catalytic Asymmetric Epoxidation of α,β-Unsaturated Esters Using an Yttrium-Biphenyldiol Complex. *J. Am. Chem. Soc.* **2005**, *127*, 8962−8963.

(14) (a) Rout, S. K.; Guin, S.; Ghara, K. K.; Banerjee, A.; Patel, B. K. Copper Catalyzed Oxidative Esterification of Aldehydes with Alkylbenzenes via Cross Dehydrogenative Coupling. *Org. Lett.* **2012**, *14*, 3982−3985. (b) Sharma, N.; Kotha, S. S.; Lahiri, N.; Sekar, G. Copper-Catalyzed One-Pot Synthesis of α-Ketoamides from 1-Arylethanols. *Synthesis* **2015**, *47*, 726−736. (c) Li, Z.; Li, C.-J. CuBr-Catalyzed Efficient Alkynylation of sp^3 C−H Bonds Adjacent to a Nitrogen Atom. *J. Am. Chem. Soc.* **2004**, *126*, 11810−11811.

(15) Henegar, K. E.; Cebula, M. Process Development for (S,S)-Reboxetine Succinate via a Sharpless Asymmetric Epoxidation. *Org. Process Res. Dev.* **2007**, *11*, 354−358.

(16) Hill, J. G.; Rossiter, B. E.; Sharpless, K. B. Anhydrous tert-butyl hydroperoxide in toluene: the preferred reagent for applications requiring dry TBHP. *J. Org. Chem.* **1983**, *48*, 3607−3608.

(17) Liu, H.; Gu, L.; Zhu, P.; Liu, Z.; Zhou, B. Evaluation on Thermal Hazard of Ter-Butyl Hydroperoxide by Using Accelerating Rate Calorimeter. *Procedia Eng.* **2012**, *45*, 574−579.

(18) Available from Sigma Aldrich Co. as a 5−6 M solution in nonane or decane.

(19) (a) Seubold, F. H.; Rust, F. F.; Vaughan, W. E. The Vapor Phase Decomposition of t-Butyl Hydroperoxide and Reactions of the t-Butylperoxy Radical. *J. Am. Chem. Soc.* **1951**, *73*, 18−20. (b) Hiatt, R.; Mill, T.; Mayo, F. R. Homolytic decompositions of hydroperoxides. I. Summary and implications for autoxidation. *J. Org. Chem.* **1968**, *33*, 1416−1420. (c) Benson, S. W.; Spokes, G. N. Very low pressure pyrolysis. III. tert-Butyl hydroperoxide in fused silica and stainless steel reactors. *J. Phys. Chem.* **1968**, *72*, 1182−1186.

(20) Andreozzi, R.; Caprio, V.; Crescitelli, S.; Russo, G. The thermal stability of tert-butyl hydroperoxide—acid mixtures. *J. Hazard. Mater.* **1988**, *17*, 305−313.

(21) Verhoeff, J. Explosion Hazards of Tertiary Butyl Hydroperoxide (TBHP). In *Runaway Reactions*; I. Chem. E. Symposium Series *68*; paper 3/T; https://www.icheme.org/communities/subject_groups/safety%20and%20loss%20prevention/resources/hazards%20archive/~/media/Documents/Subject%20Groups/Safety_Loss_Prevention/Hazards%20Archive/S068%20-%20Runaway%20Reactions/S68-18.pdf (accessed Feb 12, 2018).

(22) Slater, C. S.; Savelski, M. J.; Moroz, T. M.; Raymond, M. J. Pervaporation as a green drying process for tetrahydrofuran recovery in pharmaceutical synthesis. *Green Chem. Lett. Rev.* **2012**, *5*, 55−64.

(23) Nonane was chosen as the solvent because commercially available TBHP in nonane (limited to 100 mL bottles) was used in process development.

(24) (a) Anderson, N. Practical Use of Continuous Processing in Developing and Scaling Up Laboratory Processes. *Org. Process Res. Dev.* **2001**, *5*, 613−621. (b) Kockmann, N.; Gottsponer, M.; Zimmermann, B.; Roberge, D. M. Enabling continuous-flow *chemistry* in microstructured devices for pharmaceutical and fine-*chemical* production. *Chem. - Eur. J.* **2008**, *14*, 7470−7477. (c) Hessel, V. Novel Process Windows − Gate to Maximizing Process Intensification via Flow. *Chem. Eng. Technol.* **2009**, *32*, 1655−1681. (d) Anderson, N. Using Continuous Processes to Increase Production. *Org. Process Res. Dev.* **2012**, *16*, 852−869. (e) May, S. A.; Johnson, M. D.; Braden, T. M.; Calvin, J. R.; Haeberle, B. D.; Jines, A. R.; Miller, R. D.; Plocharczyk, E. F.; Rener, G. A.; Richey, R. N.; Schmid, C. R.; Vaid, R. K.; Yu, H. Rapid Development and Scale-Up of a 1H-4-Substituted Imidazole Intermediate Enabled by Chemistry in Continuous Plug Flow Reactors. *Org. Process Res. Dev.* **2012**, *16*, 982−1002. (f) Teoh, S. K.; Rathi, C.; Sharratt, P. Practical Assessment Methodology for Converting Fine Chemicals Processes from Batch to Continuous. *Org. Process Res. Dev.* **2016**, *20*, 414−431. (g) Porta, R.; Benaglia, M.; Puglisi, A. Recent Developments in the Synthesis of Pharmaceutical Products. *Org. Process Res. Dev.* **2016**, *20*, 2−25. (h) Movsisyan, M.; Delbeke, E. I. P.; Berton, J. K. E. T.; Battilocchio, C.; Ley, S. V.; Stevens, C. V. Taming hazardous chemistry by continuous flow technology. *Chem. Soc. Rev.* **2016**, *45*, 4892−4928. (i) Guo, S.; Dai, Z.; Hua, J.; Yang, Z.; Fang, Z.; Guo, K. Microfluidic synthesis of α-ketoesters via oxidative coupling of acetophenones with alcohols under metal-free conditions. *React. Chem. Eng.* **2017**, *2*, 650−655. (j) Gutmann, B.; Cantillo, D.; Kappe, C. O. Continuous-Flow Technology — A Tool for the Safe Manufacturing of Active Pharmaceutical Ingredients. *Angew. Chem., Int. Ed.* **2015**, *54*, 6688−6728.

(25) (a) Van Alsten, J. G.; Reeder, L. M.; Stanchina, C. L.; Knoechel, D. J. Continuous Reaction/Crystallization Process for Production of a Hazardous Intermediate. *Org. Process Res. Dev.* **2008**, *12*, 989−994. (b) Kulkarni, A. A.; Kalyani, V. S.; Joshi, R. A.; Joshi, R. R. Continuous Flow Nitration of Benzaldehyde. *Org. Process Res. Dev.* **2009**, *13*, 999−1002. (c) Baumann, M.; Baxendale, I. R.; Martin, L. J.; Ley, S. V. Development of fluorination methods using continuous-flow micro-reactors. *Tetrahedron* **2009**, *65*, 6611−6625. (d) Baxendale, I. R.; Ley, S. V.; Mansfield, A. C.; Smith, C. D. Multistep Synthesis Using Modular Flow Reactors: Bestmann−Ohira Reagent for the Formation of Alkynes and Triazoles. *Angew. Chem., Int. Ed.* **2009**, *48*, 4017−4021. (e) Li, B.; Widlicka, D.; Boucher, S.; Hayward, C. M.; Lucas, J.; Murray, J.; O'Neil, B.; Pfisterer, D.; Samp, S.; Van Alsten, J.; Xiang, Y.; Young, J. Telescoped Flow Process for the Syntheses of N-Aryl Pyrazoles. *Org. Process Res. Dev.* **2012**, *16*, 2031−2035.

(26) Safety testing confirmed that the TBHP solution in nonane was stable in stainless steel containers under ambient temperature storage.

(27) E-factor = kg of waste/kg of product. Previous process: E(previous) = 27 270 kg of waste/14 kg of product = 1948. Modified (current) process: E(current) = 17 550 kg of waste/134 kg of product = 131.

(28) https://www.lyondellbasell.com/globalassets/documents/chemicals-technical-literature/t-hydro-product-safety-bulletin-3453.pdf (accessed Feb 12, 2018).

DOI: 10.1021/acs.oprd.8b00083
Org. Process Res. Dev. 2018, 22, 707−720